GAP JUNCTION STRUCTURES

II. Analysis of the X-Ray Diffraction Data

LEE MAKOWSKI, D. L. D. CASPAR, W. C. PHILLIPS, and D. A. GOODENOUGH

From the Rosenstiel Basic Medical Sciences Research Center, Brandeis University, Waltham, Massachusetts 02154 and the Department of Anatomy, Harvard Medical School, Boston, Massachusetts 02115

ABSTRACT

Models for the spatial distribution of protein, lipid and water in gap junction structures have been constructed from the results of the analysis of X-ray diffraction data described here and the electron microscope and chemical data presented in the preceding paper (Caspar, D. L. D., D. A. Goodenough, L. Makowski, and W. C. Phillips. 1977. 74:605–628). The continuous intensity distribution on the meridian of the X-ray diffraction pattern was measured, and corrected for the effects of the partially ordered stacking and partial orientation of the junctions in the X-ray specimens. The electron density distribution in the direction perpendicular to the plane of the junction was calculated from the meridional intensity data. Determination of the interference function for the stacking of the junctions improved the accuracy of the electron density profile. The pair-correlation function, which provides information about the packing of junctions in the specimen, was calculated from the interference function. The intensities of the hexagonal lattice reflections on the equator of the X-ray pattern were used in coordination with the electron microscope data to calculate the two-dimensional electron density projection onto the plane of the membrane. Differences in the structure of the connexons as seen in the meridional profiles and equatorial projections were shown to be correlated to changes in lattice constant. The parts of the junction structure which are variable have been distinguished from the invariant parts by comparison of X-ray data from different specimens. The combination of these results with electron microscope and chemical data provides low-resolution three-dimensional representations of the structures of gap junctions.

The structural variations detailed in the preceding paper (5) establish that we are looking at not one structure of the gap junction, but at a family of structures. By observing closely related states of a molecular assembly, it is often possible to infer something about the way that transitions occur between states. These molecular rearrangements may be significant in the functional activity of the structure. Furthermore, polymorphism provides a constraint on the interpretation of the diffraction patterns. For example, the connexon structure is likely to be similar in arrays with different lattice constants, although the intensities in the X-ray patterns may be quite different.

From analysis of the X-ray intensity measurements, the distribution of scattering density within the gap junction can be determined. Protein, lipid, and water have distinguishable scattering densities. The electron density of hydrated protein and lipid polar groups is about 0.40 $e/Å^3$ (electrons per cubic angstrom), that of lipid hydrocarbons is about 0.27 $e/Å^3$, and that of water is 0.33 $e/Å^3$. It is, therefore, possible to use scattering density maps to distinguish the spatial distribution of the principal chemical constituents within the junction. In this way, the diffracted X-ray intensity measurements can be used to relate the morphological features observed in the electron micrographs to the chemical composition of the junctions.

Disorder in the gap junction lattice limits the structural detail that can be seen by crystallographic analysis of X-ray diffraction patterns or electron micrographs. Averaging over many identical units results in images that are blurred by disorder. The effect of disorder in any periodic array on its X-ray or electron diffraction pattern or on the optical diffraction from an electron micrograph is to reduce the intensity of higher-angle reflections. Beyond some limiting resolution determined by the average distance that the units are irregularly displaced, reflections disappear into the diffuse scattering background from the disordered structure. Since each reflection may be considered a piece of information about the structure, a reduction in the number of observed reflections corresponds to a loss of information about the structure.

Electron microscope images of individual macromolecular units can be obtained, but only at a radiation dose that destroys the biological structure. What is usually looked at in an electron micrograph is a stained fossil or a cast of the structure. With low electron doses which yield very faint, noisy micrographs, Unwin and Henderson (14) obtained high-resolution images of the protein in the two dimensionally crystalline purple membrane by averaging over many units as is done with X-ray crystallography. They obtained the phase information that is lost in a diffraction pattern from the averaged image of the ordered structure. Electron diffraction patterns that we have recorded from gap junctions under low dose conditions do not, however, extend to the resolution of the X-ray diffraction patterns; no more than two or three reflections were observed. The X-ray diffraction patterns presented in the preceding paper provide the highest-resolution structural information that we have been able to obtain about the arrangement of protein and lipid in the gap junction.

Lack of phase information in the X-ray diffraction patterns themselves does not present a significant problem in the analysis of the gap junction structure. At the resolution at which we are working, sufficient information can be obtained from a combination of electron microscopy and *a priori* knowledge of bilayer structure to reliably phase the data. The principal reason why a phase problem does not arise is the small amount of data. All possible phase choices can be used to calculate structures which can then be checked for consistency with the electron microscope images. The major problem in the data analysis is the measurement of the diffracted intensity. In order to extract the signal from the noise in the X-ray patterns and to reliably separate meridional and equatorial diffraction, methods were used which were developed originally for image analysis of electron micrographs and for signal processing in electrical engineering. These methods provided a way of extracting information about the structure from diffraction patterns of disoriented gap junction specimens in which there is a significant amount of disorder.

The use of results from X-ray diffraction, electron microscopy, and chemical analysis together to characterize the structure provides more information than simply adding up conclusions derived independently from the different techniques. The X-ray scattering density maps, calculated using constraints from electron micrographs, imply a distribution of lipid and protein that must be there in the proportions indicated by the chemical analyses. Requiring that the interpretations of the different bits of information about the structure be self-consistent reduces the ambiguities inherent in the separate observations.

MATERIALS AND METHODS

Isolation of gap junctions from mouse liver, electron microscopy, and X-ray diffraction were carried out as reported in the preceding paper (5).

The X-ray photographs were densitometered with an Optronics rotating drum scanner (Optronics International, Inc., Chelmsford, Mass.). Optical densities were usually measured on a 100 μm raster, although a 25 μm raster was occasionally used. The resulting square grid of optical density measurements was averaged over 10° arcs at constant radius from the center of the diffraction patterns, producing a set of data on a polar grid. Back-

ground was estimated from the optical density measured at the positions of the zeros of meridional diffraction. When overlap of meridian and equator was significant, contributions from the two could often be separated by recognition of the distinctive peak shapes of the two sources of diffracted intensity. Where ambiguities in background determination arose, the optical densities at a given radius from the center of the diffraction pattern were analyzed as a function of angle about the center of the pattern. Angular deconvolution of the data for a disorientation function was occasionally used, but could provide reliable background determination only on the very best oriented specimens.

After background subtraction, the continuous diffraction on the meridian was corrected for disorientation and the Lorentz factor by multiplying the measured intensities by the square of the reciprocal space radius $R = 2\sin\theta/\lambda$, where 2θ is the angle of scattering and λ is the wavelength of the X rays used (1.54 Å). The absolute value of the continuous transform was obtained by taking the square root of the resultant,

$$|F(R)| = \sqrt{R^2 I(R)},$$

where $I(R)$ is the background corrected signal. The structure factors for the equatorial reflections were obtained in a similar manner, first correcting the reflections for multiplicity (a_{hk}), as well as disorientation and the Lorentz factor (R^2),

$$|F_{hk}| = \sqrt{R^2 a_{hk} I_{hk}},$$

where a_{hk} is the multiplicity correction for the reflection (h, k),

$$a_{hk} = \begin{cases} 1 \text{ when } h = 0 \text{ or } k = 0 \text{ or } h = k \\ 1/2 \text{ Otherwise} \end{cases}$$

In these equations, one factor of R is due to disorientation, and one is the Lorentz factor.

ANALYSIS OF X-RAY DATA

Meridional Diffraction

Meridional diffraction is due to electron density fluctuations perpendicular to the plane of the gap junction, and complete analysis of this diffraction leads to the calculation of the one-dimensional electron density distribution along this direction. Some diffraction photographs were of sufficient quality to allow the calculation of the interference function and the pair-correlation function of the junctions stacked in the sample. As mentioned in the preceding paper (5), significant differences in meridional diffraction were observed among different specimens. In this section, the complete analysis of the meridional diffraction from specimen E153 is described. In later sections, the meridional diffraction from different specimens will be compared.

A densitometer trace of the meridional diffraction from specimen E153 is shown in Fig. 1. The modulus of the continuous transform, $|F|$, is determined by subtraction of background and correction for geometric factors. In order to calculate the electron density profile from this function, the continuous transform must be phased, and its value at very small diffraction angles must be determined. More accurate calculation of the electron density profile can be made by correcting the data for interference effects due to the stacking of junctions in the specimen. This correction also leads to an estimate of the pair-correlation function for the junctions in the specimen.

The background was subtracted by assuming that the minima of the meridional diffraction are nodes of the transform. That this is, in fact, the case can be shown by the minimum wavelength principle as discussed below. Only two ambiguities arise in this procedure. Assuming that the minimum of about 0.04 $Å^{-1}$ is a zero leads to an unexpected "bump" in an otherwise monotonically decreasing background. By plotting the optical density (which has been measured on a polar grid relative to the center of the diffraction pattern) as a function of angle at this radius on the diffraction photograph, it was found that both the meridian and equator were minima of optical density. The maximum at this radius corresponds to the position of a lattice line associated with the (1,0) or (2,0) reflection. The bump can be seen in the background on both meridional and equatorial densitometer traces and is clearly due to an off-equatorial diffraction peak. The presence of this off-equatorial peak lowers the reliability of the background subtraction in its neighborhood, but since its profile must be smooth and its magnitude is relatively low, the errors related to its presence are not likely to be too great. The other ambiguity in background subtraction is in the region of very low intensity centered at 0.06 $Å^{-1}$. Here, the noise in the data is comparable to the diffracted intensity and choice of background may be in error by an amount corresponding to the estimated signal. The question as to how many nodes there are in this region of the diffraction pattern presents the only ambiguity in phasing, and the phase choices could be biased by the way the background is subtracted.

Choosing phases for the meridional diffraction

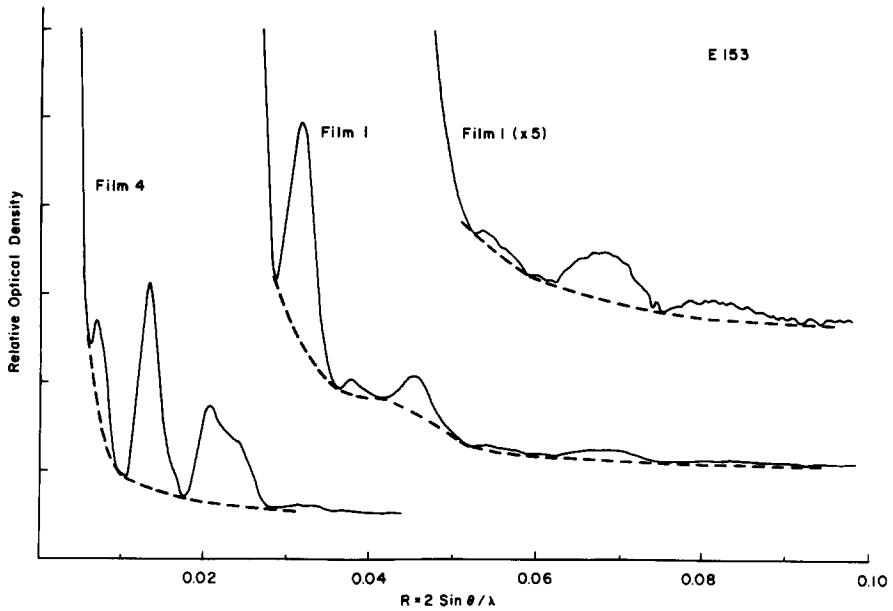

FIGURE 1 Densitometer trace of the meridian of the X-ray diffraction pattern from specimen E153 shown in Fig. 10*a* of the preceding paper. The reciprocal space coordinate R is defined in terms of the scattering angle 2θ, and the wavelength λ of the X-rays used which was 1.54 Å. At small scattering angles, the distance, R, is simply proportional to distance measured on the film. The optical densities were measured on a 100-μm grid for Film 1 and a 25-μm grid for Film 4, and then averaged on arcs $\pm 5°$ from the meridian. Four films were exposed simultaneously. Since each film absorbs about 30% of the incident radiation, Film 1 receives about 27 times the exposure of Film 4. This allows measurement of a wide range of intensities with a single exposure. Traces taken from Film 4 and Film 1 are shown. In order to show the high-angle detail, the intensity scale on the tracing from Film 1 is magnified ($\times$ 5) in the third trace shown. The broken line represents the background drawn to connect the minima identified as zeros of the junction transform.

once the background is subtracted is relatively straightforward. Since the gap junction is centrosymmetric, the transform must be a real function, and the phase choice is reduced to a sign choice. The minimum wavelength principle (3) is sufficient to determine the sign relations among adjacent peaks. According to this principle, two adjacent peaks in the diffraction from a centrosymmetric structure of lateral extent, d, in real space must be of opposite sign if the peak separation in reciprocal space is less than $2/d$. Electron micrographs of gap junctions show that the width is about 150 Å; therefore, any two diffraction peaks closer than (1/75) $Å^{-1}$ to each other must be of opposite sign. This condition requires a sign change at all observed minima in the intensity except the region of low intensity about 0.06 $Å^{-1}$. There is clearly a zero at about 0.052 $Å^{-1}$. Between 0.058 $Å^{-1}$ and 0.062 $Å^{-1}$ there may be one or two zeros. Close inspection of the densitometer traces suggests that two is most likely. However, since the magnitude of the noise in this region is comparable to the intensity of diffraction, a more reliable demonstration is necessary. The number of zeros in this region is important since it will affect the assignment of signs for the last two diffraction fringes. These fringes contribute significant high-resolution detail to the calculated density profile.

Knowledge of the width of the junction was used to resolve the ambiguity about the number of zeros in the region about 0.06 $Å^{-1}$ in the diffraction pattern. The electron density profiles for the two possible choices of signs were calculated. These profiles were truncated at ± 90Å from the center since the maximum thickness of the junction is definitely less than 180 Å. The diffraction pattern was recalculated from the truncated profiles. The truncation removes the contribution of high spatial frequency noise and interference effects in the diffraction pattern. Comparison of the recalculated intensity with that measured showed

that the structure corresponding to only one zero in this region would give rise to diffraction much stronger than that actually detected at spacings of about 0.06 $Å^{-1}$. Only the choice of two zeros was consistent with the observed intensity. Neither the uncertainties in measurement of background nor the presence of interference effects substantially affect this analysis. In this region of the pattern, diffracted intensity is hardly greater than background; thus background is accurately measured. Interference is a multiplicative effect which is negligible in regions of low intensity. We conclude from this analysis that there are two zeros between 0.058 and 0.062 $Å^{-1}$.

The central maximum must be positive since the density of the gap junction is greater than that of water. All phase relationships between adjacent peaks have therefore been established out to a spacing of 0.1 $Å^{-1}$. The phasing of the meridional diffraction determined by these methods is shown in Fig. 2.

The central maximum was measured into a spacing of 0.0042 $Å^{-1}$ using a long camera (300 mm specimen-to-film distance). The central maximum was then extrapolated into zero angle using the Shannon sampling theorem (11). Care was taken to insure that the interference effects discussed below did not affect this estimate. With the sign choice in Fig. 2, the electron density profile shown in Fig. 3 was calculated using the extrapolated central maximum.

The measured X-ray diffraction intensity is, in general, the product of a term containing information about the structure of the scattering unit and a term due to interference of diffraction from different scattering units in the specimen. The properties of the interference function are discussed in the appendix. Interference introduces higher spatial frequencies into the diffraction pattern than would be present in diffraction from a single unit. Examination of the electron density profile in Fig. 3 shows that significant ripple is present at dis-

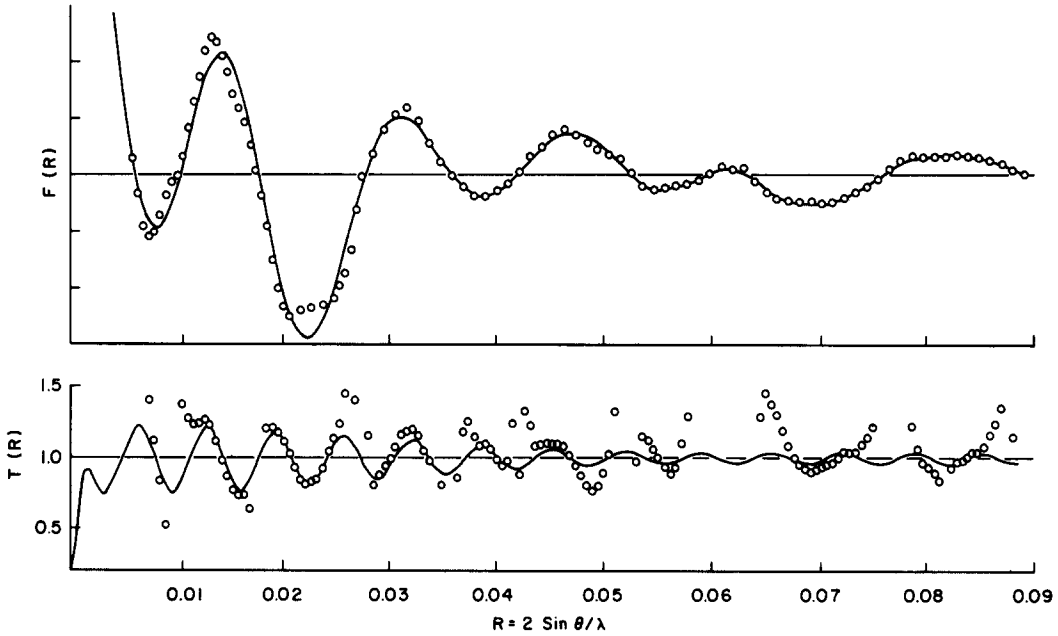

FIGURE 2 Meridional diffraction amplitude and Fourier transform of the membrane electron density profile corrected for interference effects. The open circles in the top graph are measured from the densitometer traces from specimen E153 (Fig. 1) and phased as described in the text. The solid line is the continuous transform corrected for the interference effects due to stacking of the junctions. This curve is the Fourier transform of the electron density profile in solid line in Fig. 3. The bottom graph, T(R), is a plot of the square root of the interference function as defined in the Appendix. This function is the ratio of the data points and continuous curve plotted above. The open circles indicate T(R) as experimentally determined. The continuous curve is the T(R) calculated from the pair-correlation function shown in Fig. 4. Since the experimental error in T(R) is inversely proportional to the magnitude of F(R), data points near the zeros of F(R) are indeterminant and have been omitted from this graph.

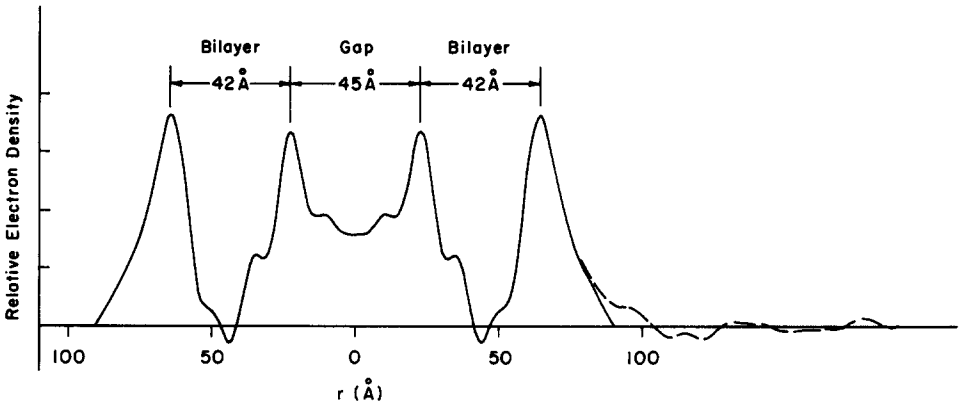

FIGURE 3 Electron density profile of gap junctions. The continuous curve is the electron density profile corrected for the interference function. The high density peaks in the electron density profile correspond to the positions of the polar groups of the bilayer lipids. The polar groups are separated by 42 Å across the bilayers and 45 Å across the gap. The low density minimum in the center of the bilayer is occupied mainly by lipid hydrocarbon and protein. The electron density of this region is much higher than would be expected for pure lipid hydrocarbons. There must be a significant protein content in this region to raise the average electron density to nearly that of water. The center of the gap has an electron density considerably greater than that of water, indicating that a significant fraction of the gap must also be occupied by protein. The electron density profile calculated directly from the data from specimen E153 is shown by the broken line. This curve differs from the corrected electron density profile only at distances greater than the thickness of the junction. The difference between these two curves is the only information available for the calculation of the interference function which is the reason for the high experimental error involved in its determination. The ripple beyond the junction boundary represents an averaged density projection of the neighboring junction units. If the stacking arrangement of junctions were crystalline, the projection of the neighboring unit would be a mirror image of the junction shown in the solid line.

tances greater than 90 Å from the center of symmetry of the junction. Some of this ripple is due to experimental error, but most of it is due to interference effects. By correcting the diffraction data for this effect, a more accurate electron density distribution may be obtained and the pair-correlation function calculated.

The interference function may be determined from electron micrographs of X-ray specimens using optical diffraction as reported in the preceding paper (5). In this study, the optical transforms were used only as a guide to aid in the evaluation of the X-ray results. In the optical transform of the tracings shown in the preceding paper, the diffraction fringes due to interference have a wavelength of about 150 Å. The interference damps out slowly, with eight or more fringes visible in strongly exposed patterns. As will be shown below, these properties are completely consistent with the interference function determined from the X-ray data.

The interference function was estimated from the X-ray data by assuming that all calculated electron density greater than 90 Å from the center of symmetry of the junction was due to interference effects as discussed in the Appendix. The electron density profile was then refined using the real space constraint that the pair-correlation function must be zero inside the interval ±140 Å about the origin. This is due to the fact that junctions, which appear to be about 150 Å across from the electron microscopy, cannot come closer than 150 Å from each other, center-to-center. The value of 140 Å was chosen for the refinement to allow for possible interleaving of the junctions and to allow for the finite resolution of the data. The refinement has little effect on the electron density profile as shown in Fig. 3. However, it results in the calculation of the interference function shown in Fig. 2 and the pair-correlation function shown in Fig. 4.

The electron density profile in Fig. 3 shows that the gap junction exhibits a typical lipid bilayer profile with the electron density elevated by a large amount of protein which spans the bilayer. The high electron density in the gap region is also indicative of high protein content in the space between membrane bilayers.

The pair-correlation function shown in Fig. 4 is sharply peaked between 150–160 Å. This indicates that the junctions in the pellet are capable of interleaving by 20–30 Å since the maximum extent of a single junction from the corrected density profile (Fig. 3) is about 180 Å. The value of the pair-correlation function at large distances from the origin should equal the number density of the junctions in the specimen. Converting this to volume density, the derived pair-correlation function indicates that about 25% of the specimen volume is occupied by gap junctions. This is consistent with the estimated water content of the centrifuge pellets.

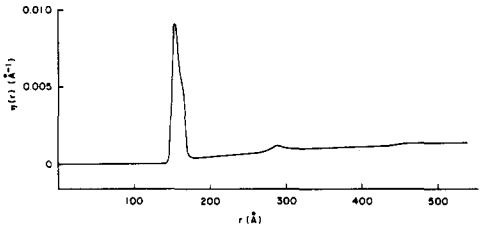

FIGURE 4 Pair-correlation function corresponding to the interference function shown in Fig. 2. The uncertainty in its determination is relatively high, but the general features are likely to be correct. The high peak at 150–170 Å indicates that pairing of junctions is a highly favored interaction. Integration of this peak shows that about 26% of junctions have a nearest neighbor between 150 and 170 Å from their center. The asymptotic value of the pair-correlation function is the number density of the specimen which is equal to 0.0014 $Å^{-1}$. To convert this to volume fraction, it is multiplied by the extent of the junctions (about 180 Å) to obtain a volume fraction of about 0.25.

Equatorial Diffraction

A densitometer trace of the equatorial diffraction is shown in Fig. 5. The hexagonal lattice of connexons in the gap junction gives rise to lattice sampling of the diffraction on the equator. The first four reflections indexed as (1,0), (1,1), (2,0), and (2,1) are much stronger than any of the others. The (1,1) and (2,0) are superimposed on a strong contribution from the meridian. The (2,1) reflection is broader than the other reflections, and shifted to a higher radius than would be expected from the positions of the other equatorial

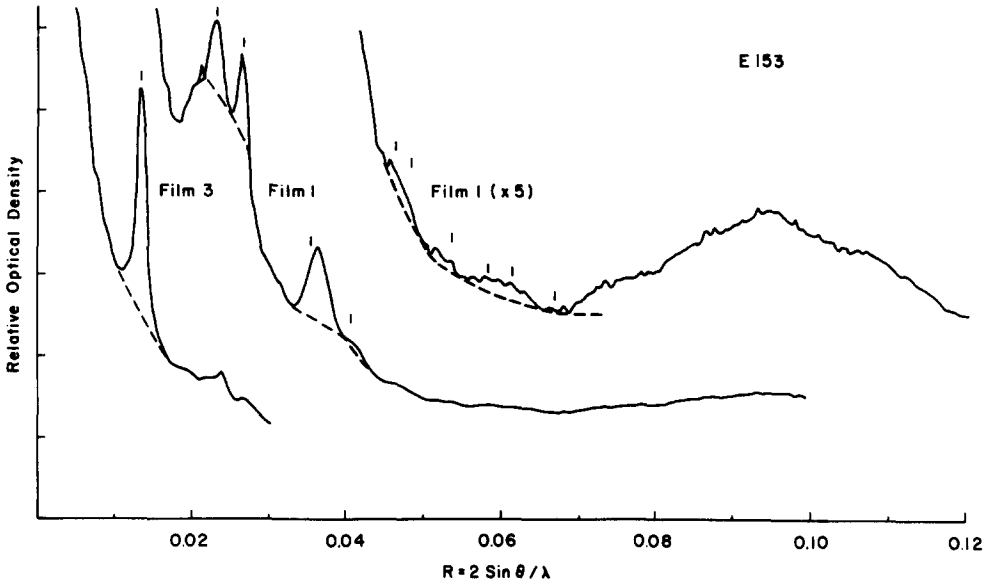

FIGURE 5 Densitometer traces of the equator of diffraction pattern from specimen E153. Optical densities were averaged on 10° arcs. Vertical bars mark the calculated positions for crystalline reflections from a hexagonal lattice with lattice constant of 86.7 Å. The background indicated by the broken line defines the crystalline diffraction maxima. The background is higher than that for the meridian due to the presence of a monochromator streak. Significant contribution of meridonal diffraction to the optical density on the equator can be seen under the (1,1) and (2,0) reflections. Although the first four orders of diffraction are easily observed, the lattice reflections at higher angles are indistinct, being replaced by a broad continuous diffraction centered at about 0.1 $Å^{-1}$. The position of the (2,1) deviates slightly from that calculated due to a significant off-equatorial contribution to the reflection.

reflections. This was a consistent property of all diffraction patterns measured, and is most probably due to strong diffraction falling slightly off the equator on the lattice line corresponding to the (2,1) reflection. A slight "bump" in the background between the (2,1) and (3,0) reflections comes from off-equatorial diffraction as discussed in the analysis of the meridional diffraction. Beyond the (3,0), the reflections are very weak and only estimates of their intensity can be made. The observed intensities from specimens E153 and F38 are plotted in Fig. 6. For the very weak, higher index reflections, an estimate of the maximum possible intensity consistent with the observed data is given. Note, however, that the intensities of some of these reflections are not significantly different from background. The minimum intensity for these reflections is zero, and the maximum is set by the noise level which determines the uncertainty in the background.

At higher angles the sampled diffraction is replaced by a broad band of continuous diffraction centered at about 10 Å spacing on the equator. This continuous diffraction is typical of diffraction from α-helices. Measurement of the optical density as a function of angle about the center of the diffraction pattern shows that the disorientation of this band is approximately the same as that from other reflections. This suggests that the band of intensity is coming from α-helices oriented within 20° of the perpendicular to the plane of the junction.

An analysis of the hexagonal lattice reflections

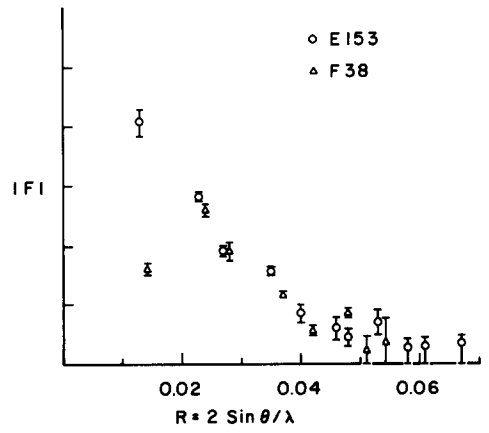

FIGURE 6 Magnitude of the structure factors of equatorial lattice reflections for specimens E153 (○) and F38 (△). The lattice constant of E153 is 86.7 Å, and of F38, 82 Å, thus the F38 reflections occur at larger spacings.

leads to the calculation of the projection of the electron density onto the plane of the junction. Electron microscopy provides a guide in the choices of phases for the equatorial diffraction. As discussed in the preceding paper, electron microscope and biochemical evidence shows that the connexon, about 30 Å in radius, is centered on the sixfold axis of the unit cell. Most of the rest of the unit cell must be made up of junction lipid. The meridional data indicate that the lipid is in a bilayer arrangement. The equatorial projection of a lipid bilayer is expected to be flat since no large-scale lateral order which could produce significant density fluctuation is likely in the lipid packing. The projected lipid density will be significantly less than that of protein. These facts provide constraints on the form of the electron density projection. It must be relatively flat outside 35 Å radius from the sixfold axis with much higher density inside that radius. Finding a phase choice that satisfies these constraints demonstrates that the equatorial X-ray pattern is consistent with other information about the structure. Furthermore, having determined the phases, the X-ray data provide information about the distribution of protein within the connexon.

The P6m symmetry of the junction in projection constrains the equatorial reflections to be real. As for the meridian, the phase choice is reduced to a sign choice, and only a few electron density projections need to be examined. For the first five reflections, all possible electron density projections were calculated. Those with unacceptable features, such as a peak on the threefold axis, were discarded, and only one phase choice was found to be consistent with all the structural constraints of the electron microscope data. The projections calculated for specimens E153 and F38 using this phase choice are shown in Fig. 7. Phase assignments for higher-order reflections were ambiguous. However, because of the very low intensities of these reflections, the projections calculated including the higher resolution data are similar to the general form of those shown in Fig. 7.

Several important features of these electron density projections are worth pointing out. First, the very low electron density at the sixfold axis was not presumed from the microscope data. It is a consistent feature of projections which satisfy the necessary constraints of the electron micrographs. Low density near the sixfold axis suggests that the protein does not fill the center of the connexon. Second, the diameter of the high den-

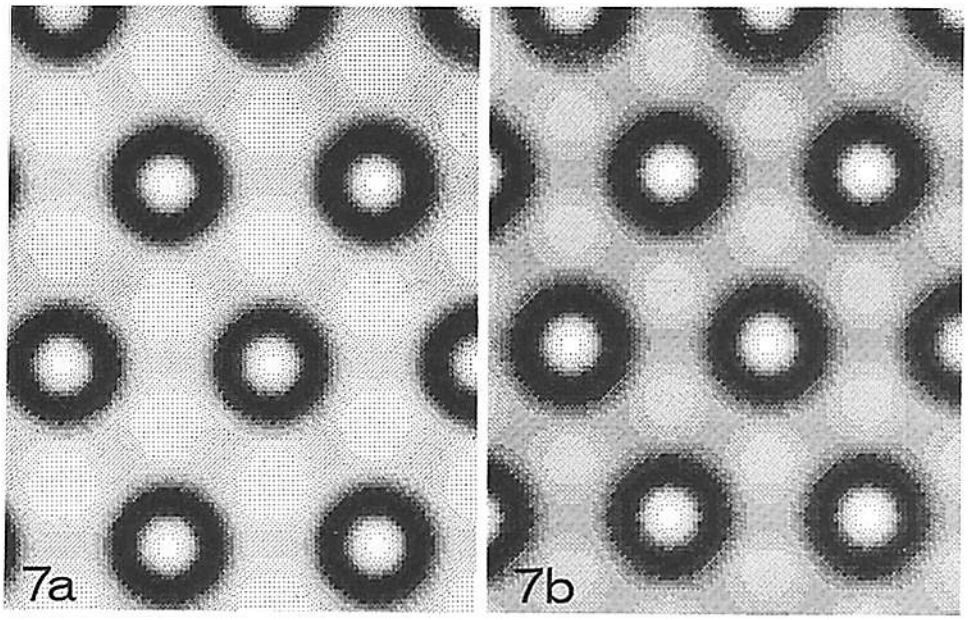

FIGURE 7 Electron density projections of specimens E153 and F38. The low-resolution projections of E153 (*a*) and F38 (*b*) were calculated from the first five reflections of the equatorial data using the phase combination (+−−−−). This is the only phase combination which produced electron density projections consistent with the structural information obtained from electron microscopy. The lattice constant of E153 is 86.7 Å; that of F38 is 82.0 Å. The data used to calculate these projections extended out to a spacing of 25 Å. In these projections, the connexons appear circularly symmetric with a diameter of about 50 Å and a low electron density core about 20 Å in radius.

sity region in these projections is less than that of the stain-excluding regions seen in micrographs. This may indicate that the diameter of the connexon in the gap region is greater than that of the portion extending through the bilayer. Finally, there is some difference between the projections from E153 and F38, suggesting a slightly different structure for the two specimens which may be correlated with the difference in lattice constant. This is particularly evident between 30 and 40 Å from the sixfold axis, where the electron density of F38 is greater than that for E153. This is more clearly illustrated in the cross sections of these projections shown in Fig. 10.

INTERPRETATION OF THE RESULTS

The Structure

The electron density profile and equatorial projection provide an accurate, low-resolution image of the gap junction ultrastructure. The profile in Fig. 3 was calculated using X-ray data extending to a spacing of about 10 Å. It shows a distribution of scattering density typical of that expected for a pair of lipid bilayers with their average electron density elevated relative to the solvent density by protein which extends through both bilayers and the extracellular gap. The high density peaks of the lipid polar head groups are separated by 45 Å across the gap and 42 Å across the bilayer. The shape of the membrane profile is very similar to that determined for pure lipid bilayers. This means that the contribution from protein to the average scattering density must be nearly constant across the width of the bilayers. The gap junction bilayer profile is asymmetric. Between the polar head group peak and hydrocarbon minimum there is a step in the electron density distribution. In the extracellular half of the bilayer, this "step" is much higher than that in the cytoplasmic half. This asymmetry may be due to a non-uniform protein distribution. However, it corresponds closely to a similar asymmetry in myelin (6) which has been attributed to an asymmetric cholesterol distribution. The higher density step in myelin is also in the extracellular half of the bilayer.

The width of the polar peak on the cytoplasmic side of the bilayer is significantly greater than that

on the extracellular surface. This suggests that additional protein may be associated with this inner surface of the membrane. The pair-correlation function shows that isolated junctions can pack with a separation of 150–160 Å. Protein on the cytoplasmic surface of the junction must be capable of interleaving with protein on adjacent junctions to make this close packing possible.

The electron density projections in Fig. 7 were calculated using data which extended to a spacing of 25 Å. In these projections, darker shading corresponds to higher average scattering density. A lipid bilayer will have a low electron density in these projections, only slightly greater than that of solvent. Thus, the dark areas are an image of the protein distribution. This image is somewhat different from the one provided by the electron micrographs of negatively stained gap junctions presented in the preceding paper (5). In the filtered images in Figs. 2 and 3 of that paper, lightly shaded areas are stain-excluding regions, and these were interpreted to correspond to the distribution of protein within the extracellular gap. These stain-excluding regions appear to occupy a much larger portion of the unit cell than the average protein distribution seen in the equatorial projections.

This combination of results from electron microscopy and X-ray diffraction suggests that the protein within the gap occupies a larger fraction of the unit cell area than it does within the bilayer. The dimensions of the protein within the gap can be estimated from the electron micrographs of negatively stained specimens. The mean diameter of the connexon spanning the bilayer can be estimated from the end on projection calculated from the equatorial diffraction data. The diameter of the connexon within the gap is 60–70 Å (Figs. 2 and 3 of the preceeding paper [5]); whereas the mean projected diameter is 50–55 Å (Fig. 7).

The end on electron density projections of the connexon have a region of low density about 20 Å in diameter centered on the sixfold axis. This corresponds to a heavily staining region in micrographs of negatively stained gap junctions. From its lower electron density, there can be little protein here. The high electron density region between 10 Å and 25 Å from the sixfold axis must contain most of the junction protein. A substantial fraction of this protein is within the lipid bilayer. Beyond 25 Å from the sixfold axis, the electron density continues to decrease to a minimum at the threefold axis. There is relatively little protein on the threefold axis, and the observed electron density there is probably mainly due to lipid and solvent. The chemical interpretation of these projections will be discussed further below.

Structural Variations

Although all the electron density profiles and projections calculated are similar, there are some significant differences. Figure 8 shows one example of these differences. This figure compares the low-resolution electron density profiles of specimens E153 and F38. Although the width of the bilayers in the two specimens is about the same, the F38 bilayer is 4 Å closer to the center of the gap than that of E153. The electron density at the middle of the bilayer is substantially larger in F38, suggesting that the protein to lipid ratio within the bilayer is greater in this specimen. F38 has a much smaller lattice constant than E153 (82 Å compared to 87 Å for E153). A larger protein to lipid

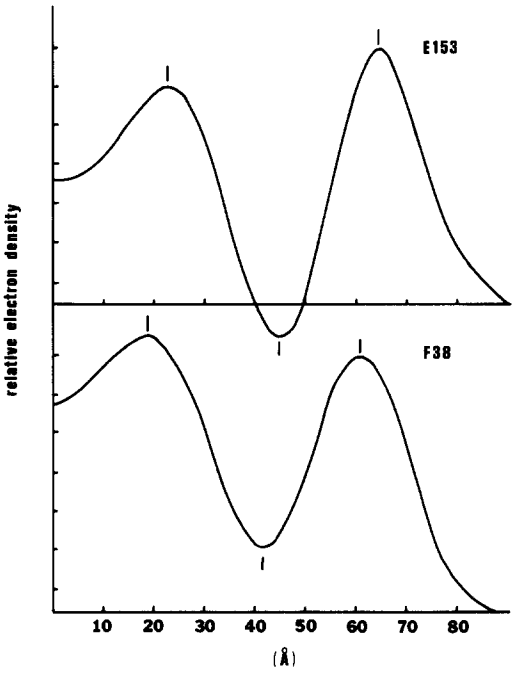

FIGURE 8 Low-resolution electron density profiles calculated from the meridians of specimens E153 and F38. The peak positions of the polar head groups are marked. Although the bilayer thickness is the same for the two specimens, the distance of the bilayer from the center of the gap is about 4 Å less for F38. The electron density at the center of the bilayer is higher in F38. This is a result of the smaller lattice constant in this specimen which is associated with a lower lipid to protein ratio in specimen F38 compared to E153.

ratio results because a decrease in lattice constant corresponds to a decrease in the lipid content of the junction if the cross-sectional area of the protein is invariant. F38 also has substantially higher electron density in the center of the gap.

By making assumptions about the electron densities of protein, lipid hydrocarbon and water, the amount of protein in the center of the gap and in the bilayer can be calculated. The electron densities assumed are 0.40 e/Å^3 for hydrated protein, 0.27 e/Å^3 for lipid hydrocarbon, and 0.33 e/Å^3 for water. Assuming that the center of the bilayer is occupied by protein and lipid hydrocarbon only, the protein content there is calculated to correspond to a protein cylinder with a radius of 26 Å for E153 and 28 Å for F38. This is consistent with the protein distributions shown in the equatorial projections in Fig. 7, and shows that, to within experimental error, the amount of protein within the bilayers of these two specimens is the same.

Assuming that only protein and water occupy the center of the gap, the same calculation can be made for this portion of the junction. The protein content in the gap corresponds to a protein cylinder about 30 Å in radius for E153 and about 39 Å in radius for F38. Examination of the electron density projection for F38 in Fig. 7, or the cross sections of this projection plotted in Fig. 10, shows that there is a high density region extending out to about 40 Å from the sixfold axis which is less pronounced in the E153 projection. The electron density profiles localize this extra density observed in the projection to the gap between bilayers. It appears that when the gap decreases in width, the protein and lipid move towards the gap as a unit and the extra protein in the gap spreads out occupying a considerably larger fraction of the gap area. The volume of protein within the gap, however, appears to remain the same.

Our X-ray diffraction measurements show that there is a strong correlation between the width of the extracellular gap and the lattice constant. In Fig. 9 the positions of the second, third, and fourth meridional zeros are plotted vs. lattice constant for 33 specimens. When the lattice constant decreases there will be an increase in the protein to lipid ratio in the junction lattice. However, this will have very little effect on the positions of the meridional zeros unless the width of the junction changes. A series of model calculations were done which indicated that the change in the positions of the meridional zeros is due to a change in the gap

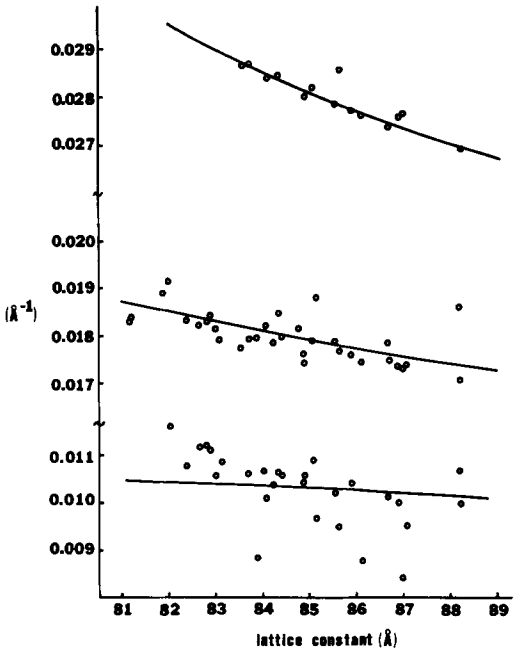

FIGURE 9 A plot of the positions of meridional zeros vs. lattice constant for thirty-three specimens. The solid lines are the results of a model building calculation described in the text. Several partially dried specimens were examined which had very low values for the position of the first meridional zero measured. These specimens are included in the figure and are responsible for the relatively broad scatter in the observed values of the position of this zero.

width. This was consistent with several electron density profiles which were calculated for specimens with different lattice constants. In the model which most satisfactorily reproduced the positions of the meridional zeros, the gap width decreased by 1 Å for every 1.3 Å decrease in lattice constant. For this model the bilayer profile was held invariant and, as the gap was narrowed, the volume of protein within the gap was maintained constant as suggested by the comparison of the E153 and F38 profiles in Fig. 8. The positions of the zeros predicted by this model are plotted in Fig. 9. There is, however, considerable scatter in the individual measurements. For example, comparing specimen F38 with E153 there is an 8 Å decrease in gap width correlated with only a 5 Å decrease in lattice constant.

Structural Models

From the X-ray diffraction, electron microscope and chemical data, models for the spatial distribu-

tion of the protein, lipid, and water in gap junction structures were constructed. The models derived for specimens E153 and F38 are shown in Fig. 10.

The chemical models were derived in the following way. The meridional profiles were put on an absolute scale by assuming that the electron density of the polar head group peak is 0.40 e/Å^3 and that that of solvent is 0.33 e/Å^3. The amount of protein in the gap and in the bilayer was determined by assuming that the gap contained only protein and water, and that the center of the bilayer contained only protein and lipid hydrocarbon. The similarity of the bilayer profile to previously derived profiles in pure lipid systems supports the assumption that the distribution of protein in the bilayer is relatively uniform across its width. Electron density extending into the cytoplasm from the bilayer surface was attributed to

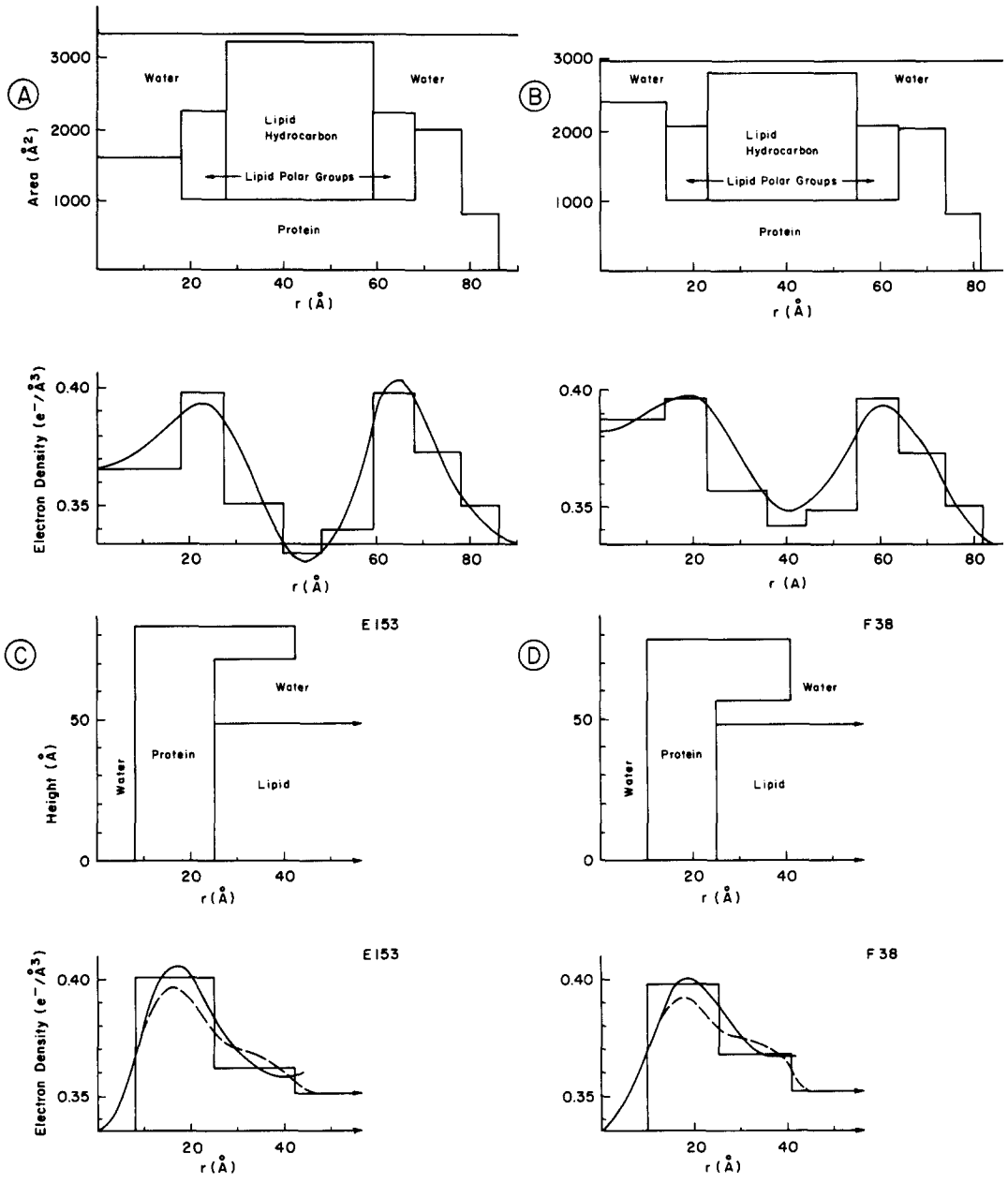

additional protein. The total protein volume was calculated to be in the range of 180–200,000 Å^3 for both specimens E153 and F38.

Similar calculations were made for the equatorial projections by assuming that the center of the connexon has the electron density of solvent and that the peak located 17–18 Å from the sixfold axis has the electron density of protein. At low resolution, cylindrically symmetric models are consistent with the electron density projections. The protein volume calculated from the equatorial projections from E153 and F38 fall in the range of 190–210,000 Å^3, consistent with that derived from the meridian.

The meridional and equatorial models were tested for consistency by comparing the total protein and total lipid volumes derived. Details of the two projections were also compared. For instance, from a comparison of meridional profiles, it was found that the electron density in the gap region of specimen F38 is much higher than that of E153. This difference corresponds to a difference in the equatorial projections of these two specimens 30–40 Å from the center of the connexon. The correspondence between these two observations presents an image of the variability of the protein distribution within the gap.

The meridional models also explain the difference in the images of the connexon in the equatorial projections and in the filtered images of negatively stained junctions. Protein occupies a larger fraction of the area in the gap than in the bilayer. The variability in the staining properties of isolated junctions (5) also appears consistent with these models. For example, there would be much less room for stain to accumulate within the gap of the junctions in specimen F38 than in specimen E153.

The protein to lipid ratio can also be calculated from the chemical models. In the models for specimen E153, the junction is 52% protein by weight and in F38 it is 57% by weight. This is consistent with the 1:1 weight ratio of protein to lipid estimated from the nitrogen and phosphorus content and the buoyant density of isolated gap junctions as reported in the preceding paper (5). The mol wt of protein in a connexon as estimated from these models is in the range of 140–170,000. If the connexon is a hexamer, it is made up of

FIGURE 10 Diagram representing the relative positions of the chemical components of gap junctions. The distribution of protein, lipid, and water perpendicular to the plane of the junctions is represented by block diagrams for specimens E153 (A) and F38 (B). The electron density profiles resulting from these distributions are superimposed on the low-resolution electron density profiles for these two specimens. The distance coordinate, r, in (A) and (B) is distance from the center of the gap measured normal to the junction plane. The elecron density of the profiles is built up from the partial areas of protein, lipid, and water for the two specimens. The absolute electron density scales are based on setting the electron density of water to 0.33 e/Å^3, of hydrated lipid polar groups and protein to 0.4 e/Å^3, and of lipid hydrocarbons to 0.27 e/Å^3. The lipids in the step regions include contribution from cholesterol and have somewhat higher electron densities. The protein content of the two specimens is the same, but the lipid content of F38 is lower because of the decrease in the area per unit cell with smaller lattice constant. In (C) and (D), the distribution of protein lipid, and water parallel to the plane of the junctions is represented by block diagrams of the chemical distribution along a line extending out from the center of a connexon. The distance coordinate, r, in (C) and (D) is radius from the sixfold axis. For simplicity, a circularly symmetric model has been constructed. The electron density projections for specimen E153 (C) and F38 (D) are built up from the partial thicknesses of the components being projected. The electron densities calculated from the chemical distributions are compared to cross sections of the electron density projections shown in Fig. 7. The smooth solid line is the electron density along a line connecting two adjacent sixfold axes in these projections. The broken line is the electron density distribution along a line connecting a sixfold axis and a threefold axis. The volume of protein in the models for both meridional profiles and both equatorial projections is the same. Although its distribution is different in the two specimens, its distribution in the profile is consistent with its equatorial projection in the individual specimens. The lipid distributions postulated for the profiles are also consistent with the projections. There is more lipid in specimen E153 than F38 because of the difference in lattice constant. From these models, the weight ratio of protein to lipid in the gap junction is about 1:1, protein accounting for 52% of the dry weight from the model for specimen E153 and 57% of the dry weight from the model for specimen F38. Thus, the distribution of chemical constituents as defined by these models is consistent with the results from measurements of nitrogen and phosphorus compositions and buoyant density reported in the preceding paper (5).

protein units with a mol wt of 23–28,000.

The structural models constructed in this way are consistent with the X-ray diffraction, electron microscope, and chemical data. Many of the conclusions of this study are summarized in Fig. 11, which is a drawing of the gap junction structures. The morphological units are composed of a dimer of hexamers of the connexin molecule; one hexamer is associated with each membrane. The hexamers form a protein tube with an outer radius of about 26 Å and an inner radius of about 10 Å. An aqueous channel extends most or all of the way through the connexon formed by the six protein molecules. The hexamers are surrounded by the lipids of the membrane bilayers. Each connexon is connected across the gap to a second hexamer, the pair making up a single morphological unit.

The protein within the gap has been observed in significantly different configurations as represented by the two drawings in Fig. 11. The protein in the gap is capable of maintaining the connection between cells over differences in gap width of at least 8 Å. The changes in gap width are correlated with changes in the average distance between connexons in the lattice.

DISCUSSION

There are two key facts about the gap junctions which must be considered in any structural study. The first is the proposed function of these structures as a pathway for intercellular communication. The second is their existence as a differentiated region of membrane which maintains chemical homogeneity and structural integrity in the fluid, heterogeneous environment of cell plasma membranes.

All evidence from physiology, electron microscopy, and X-ray diffraction is consistent with the existence of an aqueous channel extending through the connexons. Physiological experiments indicate that these channels are open to passage of small molecules between cytoplasms, but that the channels can close in response to changes in the cell environment (1). Indeed, it seems necessary for the survival of the organism that the junctions be able to seal in response to changes in cytoplasmic conditions, e.g., the death of one of the adjoining cells. Electron microscopy and X-ray diffraction data indicate that the channel is 8–10 Å in radius, but cannot demonstrate the continuity of the channel over the entire width of the junction. Electron microscopy has revealed structural changes in the large subunit gap junctions of the crayfish that are correlated with the state of electrical coupling between cells (10). These studies show that when the junctions were subject to conditions which resulted in uncoupling, the gap width and lattice constant of the junctions decreased. This was accompanied by an increase in the curvature of the junction membranes. The similarity between these observations and the structural variations observed by X-ray diffraction

FIGURE 11 Gap junction structures. These drawings illustrate the variation in the junction structure revealed by X-ray diffraction studies. The upper drawing corresponds to specimen E153 with an 87-Å lattice constant, and the lower to specimen F38 with an 82-Å lattice constant. The 42 Å dimension for the membrane bilayer thickness corresponds to the separation of the peaks in the electron density profiles, which mark the mean positions of the lipid polar groups. The overall thickness of the bilayer is about 10 Å greater. The gap in F38 is 8 Å smaller than that in E153 as measured from the electron density profiles. The 60-Å diameter connexons are hexamers of a protein molecule about 80 Å long and 20 Å wide. The protein subunits of each connexon are arrayed to form an axial channel with a maximum diameter of about 20 Å. The sectioned view of the connexon indicates that the portion of the protein traversing the bilayer is somewhat narrower than the ends of the molecule on the cytoplasmic and extracellular sides. Cooperative variations in the side-to-side distances between connexons in the lattice are linked to changes in the gap separation. Conformational changes appear to occur in the part of the protein spanning the gap while the interior portions of the connexon molecule seem to be relatively invariant. Changes in lattice constant of 5 Å and more require either highly flexible links between the protein molecules or indirect coupling through the lipid phase. Protein-protein contacts have not been illustrated since there is no direct evidence for such interactions. The connexon units which traverse the pair of membranes are shown floating in the two-dimensional lipid layers. This representation of the gap junction membrane structure can be viewed as a liquid crystalline version of the fluid mosaic model for cell membranes. The bilayer structure in the gap junction is very similar to that seen by X-ray diffraction in other membranes. The coordinated conformational changes in the connexon at the level of the gap, schematically illustrated in the drawings, could be related to the regulation of intercellular communication.

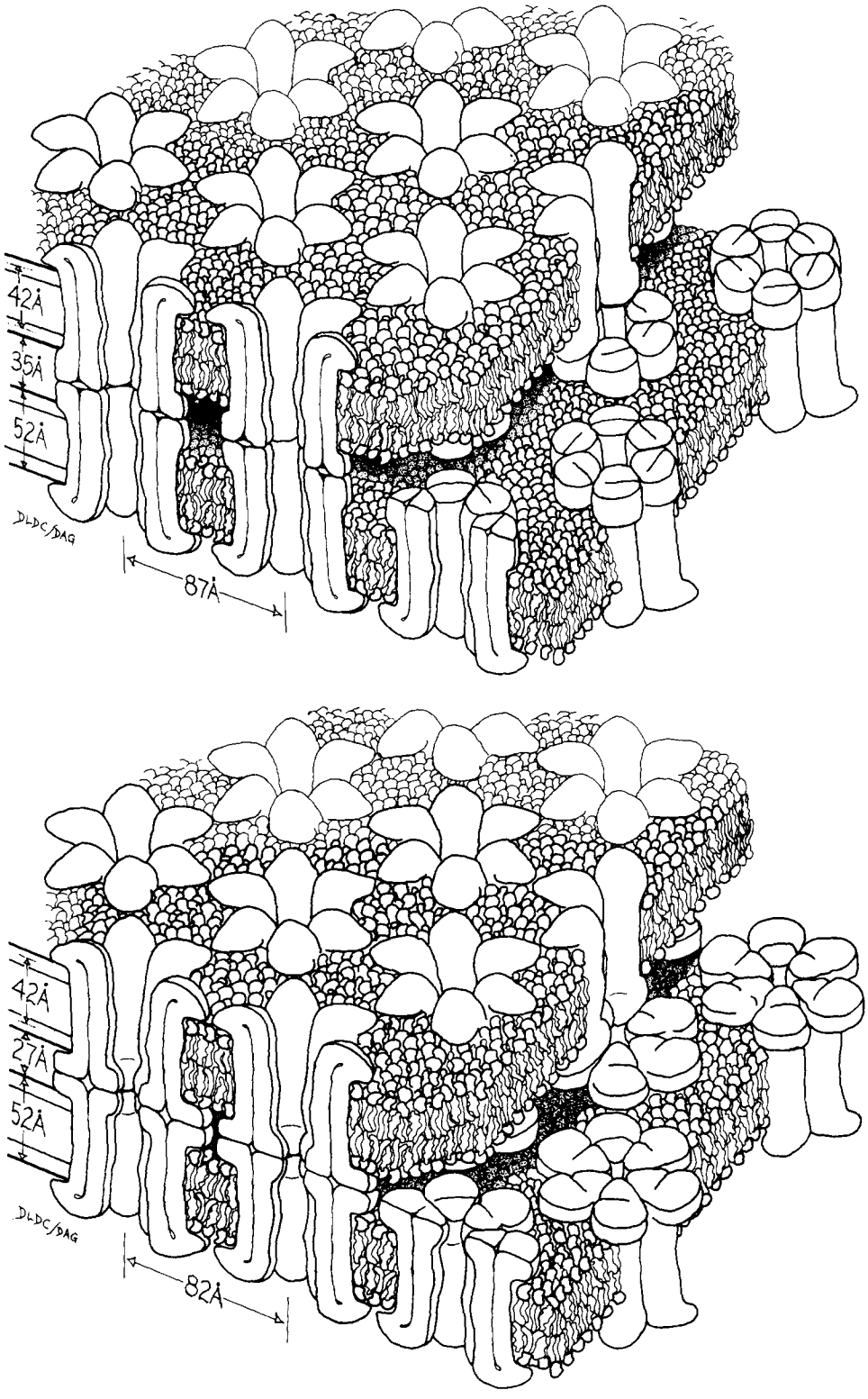
42Å
35Å
52Å
DLDC/DAG
87Å
42Å
27Å
52Å
DLDC/DAG
82Å

is striking. In spite of the very different size of the crayfish junctions and mouse liver junctions (the lattice constant and gap width of the crayfish junctions are about double those of mouse liver), they appear to undergo similar molecular rearrangements.

The contraction of the lattice implies displacement of lipid from the junction. The lipid molecules appear to act much like water molecules in crystals of soluble proteins. It is often possible to change the lattice constants of protein crystals by variation of the water activity (see, e.g., references 2 and 3). The contraction of the gap junction lattice requires the removal of lipid molecules from the array either by flow in the plane of the membrane or by movement out of the membrane. In isolated junctions where detergent is present at some stages of the isolation procedures, either process may be occurring. The movement of lipid out of the membrane when detergents are not present is energetically unfavorable, and, in the contraction of the crayfish junction lattice observed by electron microscopy, it seems likely that lipid removal occurs by movement within the plane. The coincident decrease in gap width and increase in membrane curvature complicates these considerations. For instance, it is not clear why a decrease in lattice constant should be correlated with a change in the connexon structure which results in a reduction in gap width. Nor is it clear why the action of trypsin should induce curvature in the mouse hepatocyte junction which is evidently a centrosymmetric structure.

The very existence of gap junctions is an exceptional case of membrane specialization. A large body of experimental evidence indicates that most membranes exist as fluid structures in which the membrane proteins are free to diffuse (e.g., references 4, 12, and 13), with perhaps only a few cytoplasmic strings attached (4, 7). The forces which maintain the junction lattice appear to be quite resilient, and during isolation survive detergent treatment which solubilizes most of the other membrane components of the liver. The simple fact that they can be isolated suggests that specific protein-protein interactions must be occurring between the connexons. For this to occur in a hexagonal lattice, the connexons must have sixfold symmetry and be rotationally ordered in the lattice. Proof of the rotational ordering would be strong evidence for specific interactions among the connexon units. The disorder in the lattice is surprisingly large for the maintenance of a specific bonding pattern. However, the tenacity of the structures has been demonstrated over lattice constant variations of 10% and gap width changes of at least 8 Å.

The coordinated use of structural and chemical methods has revealed that the connexon is a cylindrical assembly of connexin molecules delineating an axial aqueous channel, with a maximum diameter of about 20 Å. Our studies have demonstrated cooperative variations in the center-to-center connexon spacing that are linked to changes in the width of the extracellular gap. The structural variations are accompanied by conformational changes in the portions of the connexin molecules within the gap. These conformational changes could be related to the molecular mechanisms which regulate intercellular communication.

APPENDIX

The measured X-ray diffraction intensity $I(R)$ is, in general, the intensity that would be observed for independently scattering units $I_u(R)$ multiplied by an interference function $S(R)$ (see, e.g., references 8 and 9):

$$I(R) = I_u(R)\, S(R). \tag{1}$$

The Fourier transform of $(S(R) - 1)$ is the pair-correlation function $\eta(r)$. $\eta(r)dr$ is the conditional probability that, given that there is a scattering unit centered ar $r = 0$, there will be another one centered in the interval $(r, r + dr)$. When the scattering unit has a spatial extent d, $\eta(r)$ will, in general, be peaked at intervals equal to or slightly larger than d. For instance, for a perfect crystal, $\eta(r)$ will be a set of δ-functions at intervals of d. For disordered crystals and fluids, the modulation in $\eta(r)$ is less pronounced, and for an ideal gas $\eta(r)$ is a constant equal to the number density.

From Eq. 1, $S(R)$ is a non-negative real function. This allows consideration of the square root of Eq. 1,

$$F(R) = F_u(R)T(R), \tag{2}$$

where $T(R) = + \sqrt{S(R)}$. In real space, Eq. 2 corresponds to:

$$\rho_c(r) = \rho_u(r) * t(r), \tag{3}$$

where $t(r)$ is the Fourier transform of $T(R)$; $\rho_c(r)$, the electron density profile calculated from the observed intensities; $\rho_u(r)$, the electron density

profile of a single unit; and where the asterisk denotes convolution. The interference effects thus distort the measured electron density profile by convolution with $t(r)$. $t(r)$ is the function, which when convoluted with itself will give $(\eta(r) + \delta(r))$, where $\delta(r)$ is the Dirac delta function. As with $\eta(r)$, $t(r)$ will be peaked at intervals of d. This will result in a distortion of $\rho(r)$ which is principally confined outside the region $\pm d/2$ about the origin.

In the present study, $T(R)$ was estimated by assuming that all calculated electron density falling outside the interval ± 90 Å was due to interference effects. The pair-correlation was assumed to be equal to zero inside ±140 Å. The second constraint originates from the fact that the smallest center-to-center distance between junctions must be equal to the width of a single junction, or not less than 150 Å. A limit of 140 Å was chosen to allow for some interleaving of the structures and the finite resolution of the data. The electron density profile and interference function were then refined by an iterative procedure. The electron density profile was set to zero outside ±90 Å from the origin, and the Fourier transform was calculated. By comparison to the data, a pair-correlation function was calculated. It was set to zero inside ±140 Å, and used to calculate back a new estimate of the electron density profile. If this profile contained significant ripple outside ±90 Å, the procedure was repeated. The result of this refinement was an electron density profile $\rho_u(r)$ and a pair-correlation function $\eta(r)$, which, when combined, reproduced the observed intensity to within experimental error.

We would like to thank W. Saunders for assistance with the photography.

This work was supported by National Institutes of Heath grant no. CA15468 (D. L. D. Caspar), National Science Foundation grant no. PCM7-10111 (D. L. D. Caspar and D. A. Goodenough), National Institutes of Health grant no. GM18974 (D. A. Goodenough) and American Heart Association grant no. 73707. L. Makowski was supported by a National Institutes of Health traineeship from National Institutes of Health grant no. GM01555 to the Department of Electrical Engineering, Massachusetts Institute of Technology.

Some of the results presented here are included in a thesis submitted by L. Makowski to the Massachusetts Institute of Technology, in partial fulfillment of the requirements for the degree of Ph.D.

Received for publication 21 May 1976, and in revised form 18 April 1977.

REFERENCES

1. Bennett, M. V. L. 1973. Function of electrotonic junctions in embryonic and adult tissues. *Fed. Proc.* **32:**65–75.
2. Boyes-Watson, J. M., and F. Perutz. 1942. X-ray analysis of haemoglobin. *Nature (Lond.).* **151:**714–716.
3. Bragg, Sir Lawrence, and M. F. Perutz. 1952. The structure of haemoglobin. *Proc. R. Soc. Lond. B. Biol. Sci.* **213A:**425–435.
4. Bretscher, M. S., and M. C. Raff. 1975. Mammalian plasma membranes. *Nature (Lond.).* **258:**43–49.
5. Caspar, D. L. D., D. A. Goodenough, L. Makowski, and W. C. Phillips. 1977. Gap junction structures. I. Correlated electron microscopy and X-ray diffraction. **74:**605–628.
6. Caspar, D. L. D., and D. A. Kirschner. 1971. Myelin membrane structure at 10 Å resolution. *Nat. New Biol.* **231:**46–52.
7. Elgsaeter, A., and D. Branton. 1974. Intramembrane particle aggregation in erythrocyte ghosts. I. The effect of protein removal. *J. Cell Biol.* **63:**1018–1030.
8. Guinier, A. 1963. X-ray Diffraction. W. H. Freeman and Company Publishers, San Francisco, Calif.
9. James, R. W. 1965. The Optical Principles of the Diffraction of X-rays. Cornell University Press, Ithaca, N. Y.
10. Perrachia, D., and A. F. Dulhunty. 1976. Low resistance junctions in crayfish: structural changes with functional uncoupling. *J. Cell Biol.* **70:**419–439.
11. Sayre, D. 1952. Some implications of a theorem due to Shannon. *Acta Crystallogr.* **5:**843.
12. Singer, S. J. 1971. The molecular organization of biological membranes. *In* Structure and Function of Biological Membranes. L. J. Rothfield, editor. Academic Press, Inc., New York. 145–222 pp.
13. Singer, S. J., and G. Nicolson. 1972. The fluid mosaic model of the structure of cell membranes. *Science (Wash. D. C.).* **175:**720–731.
14. Unwin, P. N. T., and R. Henderson. 1975. Molecular structure determination by electron microscopy of unstained crystalline specimens. *J. Mol. Biol.* **94:**425–440.